The SMC5/6 complex is required for maintenance of genome integrity upon APOBEC3A-mediated replication stress

David R. O'Leary*[1,2], Ava R. Hansen*[1,2], Dylan F. Fingerman*[1,2], Thi Tran[1,2], Brooke R. Harris[1,2], Katharina E. Hayer[3,4], Mithila Tennekoon[2,5], Rachel A. DeWeerd[1,2], Alice Meroni[2,5], Julia H. Szeto[3], Matthew D. Weitzman[3,6], Ophir Shalem[7], Jeffrey Bednarski[1,2], Alessandro Vindigni[2,5], Abby M. Green[1,2†]

[1]*Department of Pediatrics, Washington University School of Medicine, St. Louis, MO, USA*

[2]*Center for Genome Integrity, Siteman Cancer Center, Washington University School of Medicine, St. Louis, MO, USA*

[3]*Division of Cancer Pathobiology, Children's Hospital of Philadelphia, Philadelphia, PA*

[4]*Department of Biomedical and Health Informatics, Children's Hospital of Philadelphia, Philadelphia, PA*

[5]*Department of Medicine, Washington University School of Medicine, St. Louis, MO, USA*

[6]*Department of Pathology and Laboratory Medicine, Perelman School of Medicine at the University of Pennsylvania, Philadelphia, Pennsylvania, USA.*

[7]*Department of Genetics, Perelman School of Medicine, University of Pennsylvania, Philadelphia, PA, USA.*

*equal contribution
†corresponding author: Abby M. Green, abby.green@wustl.edu

ABSTRACT

Mutational patterns consistent with the activity of the APOBEC3 cytidine deaminases are evident in more than half of human cancer genomes. APOBEC3-mediated mutagenesis is genotoxic when uncontrolled due to accumulation of base mutations, replication stress, and DNA breaks. In particular, the APOBEC3A family member is a potent enzyme with nuclear localization that causes substantial DNA damage in experimental systems and human tumors. However, the spectrum of genome-protective mechanisms that ensure genome stability in cells with active APOBEC3A is unknown. Through a genome-wide functional screen, we identify the Structural Maintenance of Chromosomes 5/6 (SMC5/6) complex as essential for cell viability when APOBEC3A is expressed. Cells depleted of SMC5/6 incurred substantial DNA damage when APOBEC3A was active, as reflected by increased DNA breaks, DNA damage signaling, and defective proliferation. We observed an absence of APOBEC3A mutagenesis in human tumors with dysfunction of SMC5/6, consistent with synthetic lethality. APOBEC3A is known to act on ssDNA at replication forks. We observed increased DNA damage in replicating cells in the absence of SMC5/6, suggestive of replication forks as a source of DNA breaks. We interrogated replication fork dynamics by DNA fiber spreading and found a consistent increase in the length of replication tracks upon APOBEC3A activity across multiple cell lines. Increased replication fork length was dependent on Primpol, consistent with a repriming mechanism downstream of APOBEC3A-induced lesions. Loss of SMC5/6 resulted in abrogation of fork elongation in cells with active APOBEC3A, along with increased DNA breaks. Our findings indicate that increased length of replication forks in response to APOBEC3A is a genome-protective response and is dependent on intact SMC5/6. Therefore, SMC5/6 may be a therapeutic vulnerability in tumors in which APOBEC3A is active.

INTRODUCTION

Cytidine deamination caused by APOBEC3 enzymes is among the most prevalent sources of endogenous mutagenesis in human cancers[1-7]. APOBEC3 enzymes catalyze the conversion of cytidine to uracil in single-stranded (ss)DNA substrates, which can result in mutations after replication or uracil excision[8,9]. The APOBEC3 enzymes function in the innate immune system to deaminate and mutate viral genomes and retrotransposons to restrict infection and retrotransposition[8-10]. Off-target or aberrant activity of the enzymes results in damage to the cellular genome[11-17]. Of the seven-member family (APOBEC3A-H), APOBEC3A is expressed in the nucleus and causes mutagenesis in experimental systems and human tumors, which can be genotoxic at high levels[5,18,19]. In cancer, this genotoxic potential can be exploited by inhibition of essential DNA damage responses. APOBEC3A targets ssDNA at replication forks, which elicits activation of replication stress responses initiated by ATR kinase signaling[20,21]. Inhibition of ATR causes abrogation of the cell cycle checkpoint, enables accumulation of mutations during DNA replication, and ultimately promotes replication catastrophe as cells move through mitosis[20,21]. Cytotoxicity of APOBEC3A activity upon ATR inhibition illustrates a synthetic lethal interaction and the essential nature of DNA damage responses in tumor cells undergoing mutagenesis. We used the synthetic lethality strategy to investigate the spectrum of DNA damage responses that are elicited by APOBEC3A. Using a genome-wide CRISPR-based screen, we determined that optimal function of the Structural Maintenance of Chromosomes 5/6 (SMC5/6) complex is essential in cells with active APOBEC3A.

SMC5/6 is a highly conserved eight-member complex comprised of SMC5 and SMC6 as well as six non-SMC element (NSMCE) proteins[22]. SMC5 and SMC6 dimers form the hinge-like backbone of the complex[23,24]. Similar to the related condensin and cohesin SMCs, SMC5/6 interacts with DNA in multiple ways. Notably, SMC5/6 can simultaneous bind ssDNA and dsDNA, and can stabilize ssDNA-dsDNA junctions[25,26]. Unique to SMC5/6 are catalytic activities conferred by the SUMO ligase subunit NSMCE2 and the ubiquitin ligase subunit NSMCE1[27,28]. While condensin and cohesin act in chromosome folding and segregation, the function of SMC5/6 in genome maintenance is less well defined. Experimental suppression of SMC5/6 as well as human syndromes

caused by germline defects in SMC5/6 result in replication and repair defects and chromosomal aberrations[29-33]. Despite these data indicating an important role for the complex in genome integrity, SMC5/6 deficiency in human cancer is poorly understood. In yeast and mammalian cells, SMC5/6 co-localizes with replication-associated proteins and nascent DNA, indicating that the complex localizes to replication structures[34-38]. Several genome maintenance roles for SMC5/6 at replication forks have been elucidated, such as regulation of fork reversal and resolution of recombination intermediates that arise due to repair of DNA lesions at impaired replication forks[39-42]. Additionally, SMC5/6 localizes to natural pausing sites at centromeres, telomeres, and ribosomal DNA even in the absence of genome damage, suggesting a role for support of replication through repetitive or fragile regions[35,43-46]. While SMC5/6 clearly interacts with replicating DNA, a role for the complex in protection of forks undergoing cytidine deamination has not been defined.

In this study, we discovered a synthetic lethal interaction between APOBEC3A activity and loss of SMC5/6. We defined the mechanism by which SMC5/6 promotes genome stability upon deaminase activity. In a panel of cancer cell lines, we found that depletion of SMC5/6 enabled APOBEC3A activity to cause high levels of DNA breaks leading to genotoxic cell death. In cells depleted of SMC5/6, deaminase-induced DNA damage was maximal during DNA replication. Intriguingly, we found that APOBEC3A activity led to an apparent increase in length of replication forks as measured by DNA fiber imaging. The increased length was dependent on Primpol, thus is likely due to bypass of APOBEC3A-mediated replication obstacles by repriming downstream of a DNA lesion. Interestingly, the increased fork length was also dependent on SMC5/6. Upon loss of SMC5/6, replication fork length returned to baseline despite APOBEC3A expression, which was associated with substantial genotoxicity. Our findings indicate that SMC5/6 is responsible for replication fork progression in cells undergoing deaminase-mediated damage. These data not only demonstrate a new mechanism by which genome integrity is maintained upon APOBEC3A activity, but also a synthetic lethal interaction that may provide opportunities for therapeutic targeting of SMC5/6 in cancer.

RESULTS

Functional genomics screen identifies SMC5/6 as essential in cells with APOBEC3A activity

To identify cellular processes that ensure genome protection from mutagenic activity of APOBEC3A, we employed a genome-wide functional screening approach. We generated lentivirus from the Brunello guide RNA (sgRNA) library which includes multiple sgRNAs for each human gene as well as non-targeting control sgRNAs[47]. We engineered THP1 (myeloid leukemia) cells with a doxycycline-inducible APOBEC3A transgene (THP1-A3A) and a constitutive Cas9 transgene (**Fig S1a**). Cells were transduced with the Brunello lentivirus library to achieve a 1:1 ratio of lentivirus:cell which enabled screening for knockout of each human gene independently within a pooled population (**Fig S1b**). Following transduction, cells were selected with puromycin, then separated into treatment (+dox) and control (-dox) groups. Viable cells were harvested at day 0 prior to dox treatment and at day 15 after dox treatment for sequencing of sgRNAs (**Fig 1a**). Sequenced sgRNAs were normalized and analyzed by three independent pipelines to generate a gene score for each gene represented in the Brunello library (**Fig S1c**). Sequencing coverage of the entire library was similar across samples, regardless of dox treatment (**Fig S1d-e**). Comparison of dox-treated versus untreated cells after 15 days revealed under-represented or absent sgRNAs, indicating genes that were negatively selected in dox-treated cells (**Supplemental Table S1**). Negative selection is interpreted as cell death due to synthetic lethality between gene loss and APOBEC3A expression. The top 250 negatively selected genes were analyzed for gene ontology which revealed biological processes clustered around DNA damage and repair, DNA and RNA metabolism, and chromosome organization (**Fig 1b**). Among the negatively selected genes were ATR and CHEK1 (**Fig 1c**), which have previously been demonstrated to be synthetically lethal with APOBEC3A expression[20,21]. Further, ATM sgRNA levels remained consistent throughout the two weeks of dox treatment indicating that loss of these genes did not impact survival of APOBEC3A-expressing cells which is consistent with prior findings[20,21] (**Fig 1c**).

Within chromosome organization, which was the most significant GO term, SMC5 and NSMCE3, two members of the eight-protein complex comprising SMC5/6, were

significantly negatively selected (**Fig 1c**). Additional SMC5/6 genes were negatively selected, though appeared lower on the list. To validate this potential synthetic lethal interaction, we depleted SMC5 in THP1-A3A cells and found that, upon APOBEC3A expression, cells were significantly less viable than controls (**Fig 1d**). Thus, the SMC5/6 complex is essential for cell viability when APOBEC3A is expressed.

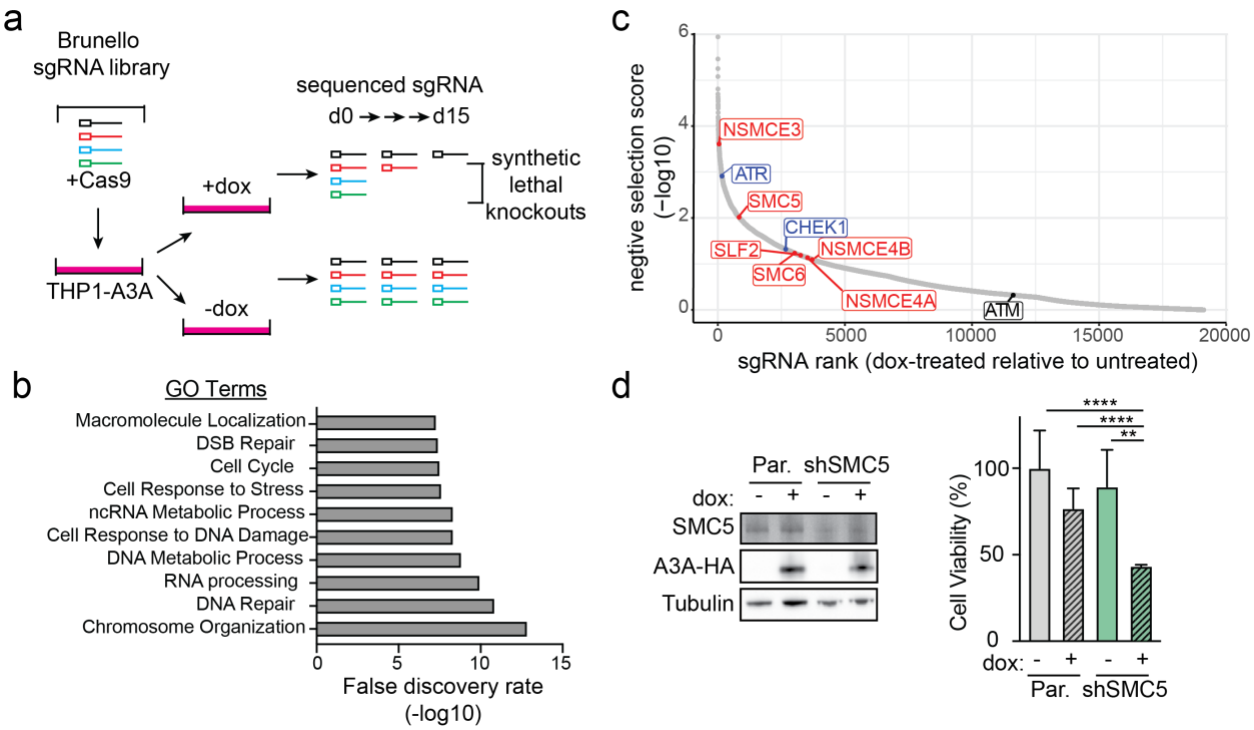

Figure 1. Functional genomics screen identifies the SMC5/6 complex as essential in APOBEC3A expressing cells. (**a**) Schematic for functional genomics screen to identify synthetic lethality with APOBEC3A. The Brunello CRISPR-Cas9 guide RNA (sgRNA) library was used in THP1 cells expressing a doxycycline (dox)-inducible, HA-tagged APOBEC3A transgene (THP1-A3A). sgRNAs were identified and quantified by sequencing at day 0 (baseline library integration) and day 15 after dox treatment. Depletion of sgRNAs at day 15 in dox-treated cells relative to untreated controls represent potential synthetic lethal genes. (**b**) The top 250 genes identified as potentially synthetic lethal with APOBEC3A are grouped by Gene Ontology (GO) terms. (**c**) Negatively selected sgRNAs in dox-treated relative to untreated cells at day 15. SMC5/6 complex genes in red. (**d**)THP1-A3A cells were depleted of SMC5 by stable integration of shRNA. Viability of cells treated with dox or untreated was determined by FACS after staining for fluorescent-labeled calcein AM (live) and DNA (dead). Cell lysates were probed with antibodies to HA and SMC5. Tubulin was used as loading control.

SMC5/6 loss potentiates APOBEC3A-mediated genotoxicity

To explore the reproducibility of a synthetic lethal interaction between APOBEC3A and loss of SMC5/6, we depleted SMC5 in cell lines from different tissue types. Prior studies demonstrated that Smc5/6 is essential in budding and fission yeast[48], and

complete deletion of SMC5/6 components was embryonic lethal in mice[49], but conditional depletion of SMC5/6 was tolerated in mammalian cells[29,50]. Thus, we turned to partial and inducible depletion of the SMC5/6 complex. In K562 (myeloid) and Jurkat (T-cell) leukemia cells, shRNAs targeting SMC5 were used for constitutive depletion of the SMC5/6 complex (**Fig 2a** and **Fig S2a**). The HCT116 colorectal carcinoma cells were engineered to constitutively express plant-derived E3 ubiquitin ligase, OsTIR1, and minimal auxin-inducible degron (mAID) tagged NSMCE4A and SMC6 subunits[29,51]. When these cells are treated with indole-3-acetic-acid (IAA) to enhance the interaction between OsTIR1 and mAID subunits, the SMC5/6 complex was degraded as previously described[29] (**Fig S2b**). K562, Jurkat, and HCT116 cells were engineered to express dox-inducible APOBEC3A transgenes. Doxycycline dose was titrated to induce a level of APOBEC3A expression that resulted in minimal DNA damage. However, in combination

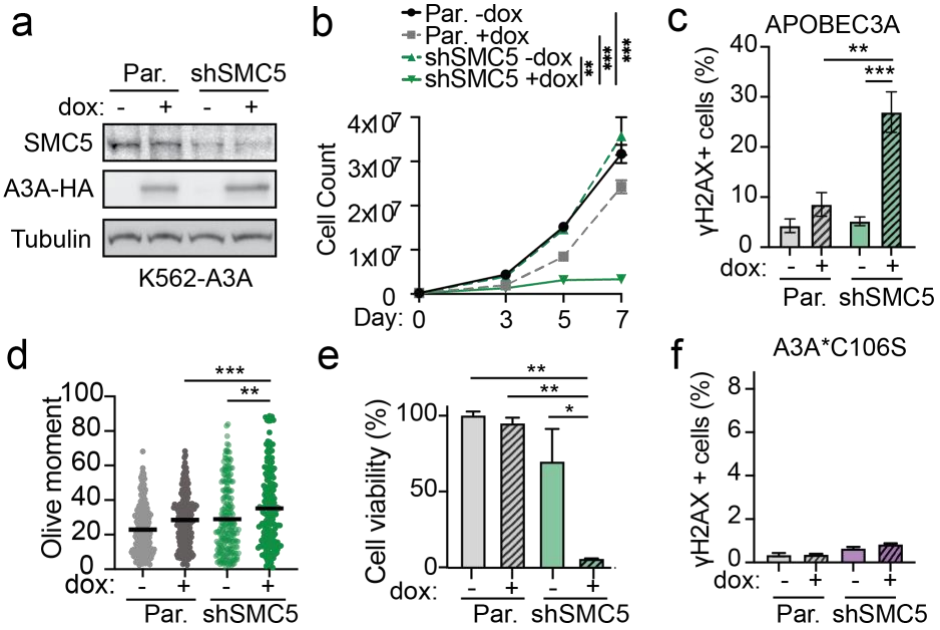

Figure 2. SMC5/6 loss potentiates APOBEC3A-mediated genotoxicity. K562 cells engineered to express doxycycline-inducible HA-tagged APOBEC3A (K562-A3A) were depleted of SMC5 by RNAi (shSMC5) and compared to parental K562-A3A cells. All results are representative of three independent biological replicates. (**a**) Immunoblot shows APOBEC3A expression (HA antibody) and SMC5 depletion. Tubulin was used as a loading control. (**b**) Cell proliferation was measured by counting cells over the course of 7 days. Bars are SEM. (**c**) DNA damage response signaling was assessed by intracellular staining and flow cytometry analysis of the phosphorylated form of the histone variant H2AX (γH2AX). Mean and SD of triplicate experiments are shown. (**d**) Comet assay results shown as dot plot of individual values, bar is median of olive moments. (**e**) Cell viability was assessed by WST8 staining of K562 cells. Mean and SD of triplicate experiments are shown. (**f**) DNA damage response signaling was assessed by intracellular staining and flow cytometry analysis of γH2AX in K562 cells expressing the catalytically inactive A3A*C106S mutant. Mean and SD of triplicate experiments are shown. p-values by two-tailed t-test. ***p<0.001 **p<0.01 *p<0.05

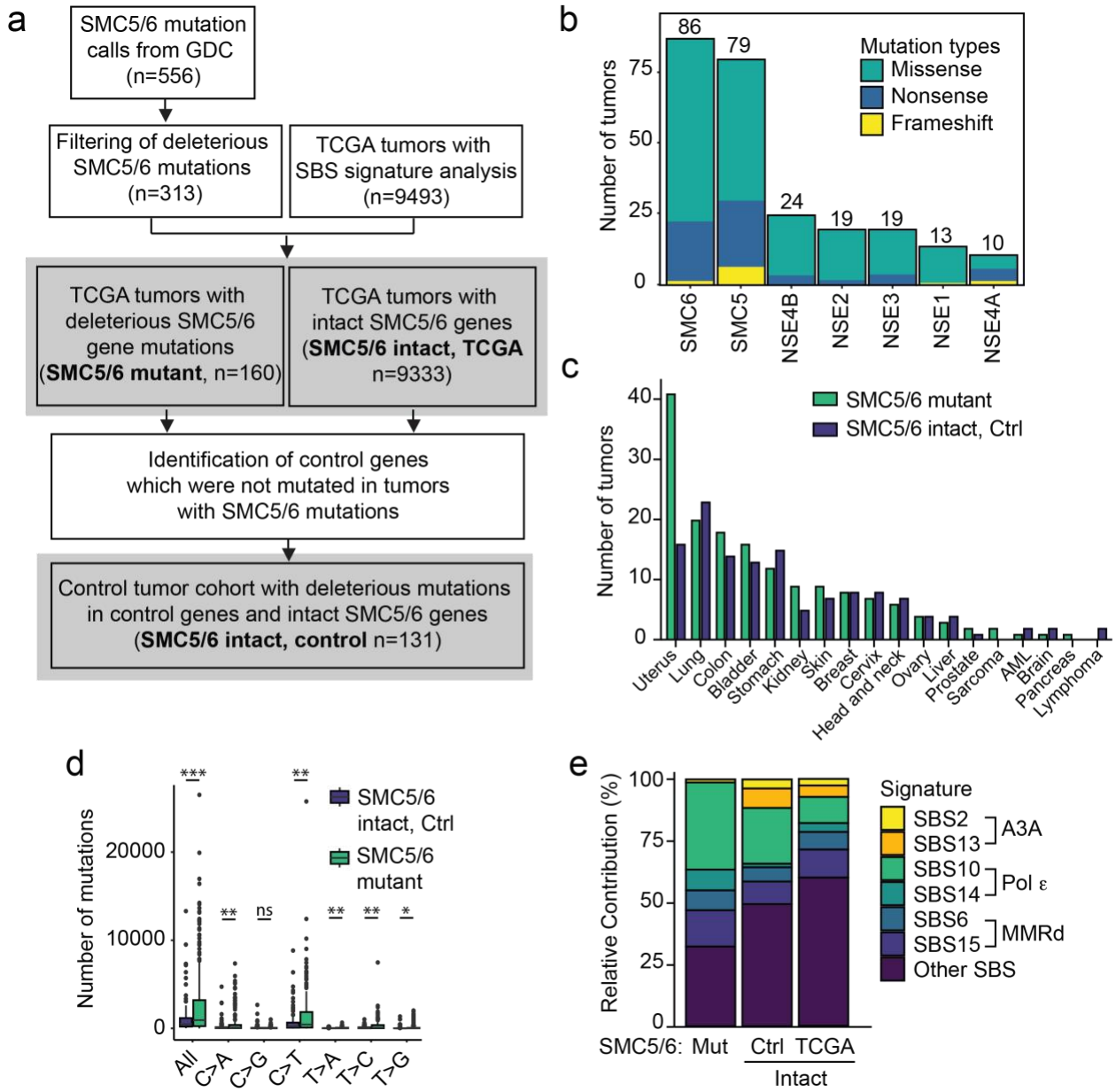

Fig 3. APOBEC3 mutational signatures are absent in tumors with dysfunctional SMC5/6. (a) Pipeline for mutational signature analysis in tumors with SMC5/6 dysfunction. Tumor genomes in the GDC data portal were evaluated for missense, nonsense, or frameshift mutations in the coding regions of SMC5/6 complex genes which would predict dysfunction. After matching with tumors in TCGA in which SBS signatures were defined, 160 tumors were identified as having mutant SMC5/6 genes. Control genes were defined by those which were never mutated in tumors with deleterious mutations in SMC5/6 genes. Tumors in which deleterious mutations in control genes were identified constituted a control (Ctrl) cohort. Bold text in gray squares indicate tumor groups included in panels **b-f**. (**b**) The number of tumors with mutations in each SMC5/6 subunit gene. (**c**) The type of tumors represented in both SMC5/6 mutant and SMC5/6 intact control groups. (**d**) Total mutation burden in each tumor genome from SMC5/6 mutant and SMC5/6 intact control cohorts. Bar is median. p-value by two-tailed t-test, *p<0.05, **p<0.01, ***p<0.001 (**e**) The relative contribution of each single base substitution (SBS) mutational signature identified within the SMC5/6 mutant (Mut) and SMC5/6 intact cohorts. The latter is divided by control cohort and all other tumor genomes within TCGA. SBS signatures that comprise >4% relative contribution to mutations within each cohort are included, along with their proposed etiology. Pol ε, polymerase epsilon; MMRd, mismatch repair deficiency.

with SMC5/6 depletion, APOBEC3A expression caused a significant proliferative defect (**Fig 2b** and **Fig S2c-d**). Additionally, we found that DNA damage response signaling was significantly increased upon APOBEC3A expression in cells depleted of SMC5 as detected by increased phosphorylation of histone variant H2AX (γH2AX), a response to DNA breaks (**Fig 2c, Fig S2e, Fig S2g**). Consistent with these results, we found an increase in DSBs by neutral comet (**Fig 2d** and **Fig S2f**). We hypothesized that increased DSBs and DNA damage resulting in poor proliferation would lead to cell death. Indeed, the culmination of genotoxicity was reflected by a decrease in viability of cells with expression of APOBEC3A and depletion of SMC5 (**Fig 2e** and **Fig S2h**).

APOBEC3A catalytic activity is required for synthetic lethality with SMC5/6 loss

We hypothesized that the synthetic lethal phenotype resulting from APOBEC3A expression and SMC5/6 loss was due to deaminase-induced genotoxicity. First, we determined that SMC5/6 depletion does not cause increased APOBEC3A deaminase activity (**Fig S3a**). If anything, deaminase activity is modestly reduced when SMC5/6 is depleted. To evaluate the requirement for deamination activity, we constructed K562 cells expressing a catalytic mutant of APOBEC3A containing a C106S amino acid change (**Fig S3a-b**). C106S expression in cells with SMC5 depletion did not result in a proliferative defect (**Fig S3c**). We found that DNA damage response signaling and DSB quantity were not significantly different when C106S is expressed, regardless of SMC5/6 status (**Fig 2f** and **Fig S3d**). These data demonstrate that deaminase activity is required for the synthetic lethal interaction between APOBEC3A expression and SMC5/6 loss.

APOBEC3A mutagenesis is incompatible with SMC5/6 dysfunction in human cancers

To evaluate the interaction of APOBEC3A activity and SMC5/6 loss in human cancers, we first identified tumors with mutations in SMC5/6 subunit genes that are predicted to be deleterious. We defined deleterious mutations as exonic missense, nonsense, or frameshift base changes. Within TCGA we found 160 tumors with deleterious mutations in SMC5/6 genes (**Fig 3a**). SMC5 and SMC6 were the most frequently mutated genes of all subunits (**Fig 3b**). For comparison, we defined a control

set of tumors with no mutations in SMC5/6 subunit genes (n=131) that were tissue-matched (**Fig 3a** and **Fig 3c**). Tumors with dysfunctional SMC5/6 had a higher overall mutation burden (**Fig 3d**), consistent with a role for the complex in genome integrity. To determine the source of mutagenesis in tumors with dysfunctional SMC5/6, we examined single base substitution (SBS) signatures. All SBS signatures (COSMIC v3.3) that comprised more than 5% contribution to mutation burden within each group of tumors are shown (**Fig 3e**). The APOBEC3A signatures, SBS2 and SBS13, comprised a substantial portion of mutations in the control tumors but were notably absent in the SMC5/6-mutant tumors (**Fig 3e**). These data support our experimental findings that dysfunction of SMC5/6 results in death of tumor cells in which APOBEC3A is active, thus the two are incompatible in viable human tumors.

SMC5/6 loss promotes APOBEC3A-mediated DNA damage during replication

It has previously been shown that APOBEC3A activity at replication forks results in mutations on both leading and lagging strands, stalled DNA replication, and activation of DNA damage signaling[11,14,15,18,20,21,52,53]. Damaged replication forks can result in replication stress and/or DNA breaks. We hypothesized that APOBEC3A activity at replication forks was a source of genotoxicity in SMC5/6-depleted cells. We examined markers of replication stress and DNA breaks by immunofluorescent cell imaging. Following degradation of the SMC5/6 complex and induction of APOBEC3A expression in HCT116-A3A cells, we observed an increase in RPA and γH2AX foci (**Fig 4a-c**). In cells with APOBEC3A expression and SMC5/6 degradation, we observed a substantial increase in co-localization of RPA and yH2AX foci compared to controls (**Fig 4d**). These data demonstrate a physical overlap between replication stress signaling and DNA break signaling, suggestive of a common location at which these genotoxic events occur.

Circumstances in which replication forks are stalled may provide more ssDNA substrate for deamination events. SMC5/6 has been implicated in perturbations and control of the G2/M cell cycle checkpoint. In plants, defective SMC5/6 promotes cell cycle progression upon DNA damage despite appropriate activation of the replication checkpoint[54]. In yeast, Nse2-mediated SUMOylation of Rqh1, a RecQ helicase, is important for replication checkpoint signaling[55]. Therefore, we evaluated cell cycle profiles

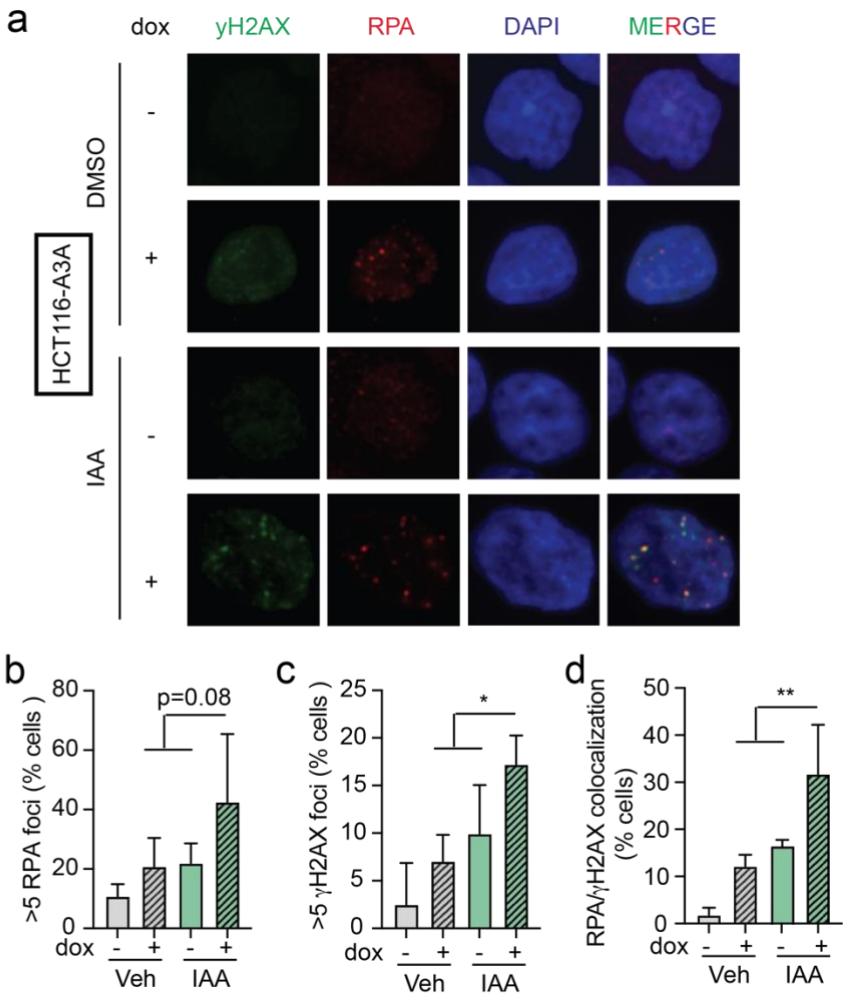

Fig 4. Replication stress and DNA break signaling co-localize in SMC5/6-depleted cells when APOBEC3A is expressed. (**a**) HCT116 cells with integrated E3 OsTIR1 ligase and mAID-tagged NSE4A and SMC6 subunits were treated with IAA to degrade SMC5/6 components and with dox to induce APOBEC3A expression for 72 hours. Representative images showing RPA foci, yH2AX foci, DAPI staining and merged images. (**b-d**) Quantification of cells with >5 RPA foci (**b**), >5 yH2AX foci (**c**), and co-localized foci (**d**). Bars are mean with SD of 3 biological replicates. 300 nuclei were analyzed per condition. p-value by nested Anova **p<0.01 *p<0.05

in SMC5/6-depleted cells to determine whether replication fork stalling could explain the exacerbated genotoxicity from APOBEC3A activity. We found that cell cycle profiles were relatively unchanged by SMC5/6 loss (**Fig S4a**). Given the exclusive activity of APOBEC3A on ssDNA substrates (as compared to dsDNA), we evaluated availability of ssDNA in cells depleted of SMC5/6. We observed that SMC5 depletion did not alter the amount of nascent ssDNA as detected by native BrdU staining (**Fig S4b**). These data show that SMC5/6 defects do not cause cell cycle arrest or increased ssDNA substrate

availability, and thus these are unlikely to explain how APOBEC3A causes excessive genotoxicity in the absence of SMC5/6.

SMC5/6 is required for APOBEC3A-mediated increase in replication fork progression

Since we found that the combination of APOBEC3A expression and SMC5/6 loss results in increased DSBs (**Fig 2**), and that sites of DSB signaling overlap with sites of replication stress (**Fig 4**), we reasoned that replication forks were the source of genotoxicity. To understand how replication forks were affected by deaminase activity upon SMC5/6 loss, we first examined the impact of APOBEC3A activity on replication fork dynamics by employing the single-molecule DNA fiber spreading assay[56]. Cells were pulsed sequentially with thymidine analogues IdU (red) and CldU (green) for a duration of 30 minutes each. After incorporation of the thymidine analogues, DNA fibers were spread, stained, and analyzed for total replication track length (IdU + CldU) (**Fig 5a**). Since the thymidine analogues are incorporated for a discreet and consistent period of time, total track length is analogous to the rate of replication fork progression[57,58]. Surprisingly, we found that APOBEC3A expression resulted in a dose-dependent increase in total track length, indicative of accelerated replication fork elongation (**Fig 5b-c**). Elongation of replication forks was dependent on deaminase activity (**Fig S5a-b**). This APOBEC3A-mediated fork elongation was observed in multiple cell types with different SMC5/6 depletion methods (**Fig 5d-e** and **Fig S5c-d**). In all cells, SMC5/6 depletion led to abrogation of replication fork elongation (**Fig 5d-e** and **Fig S5c-d**). Interestingly, the conditions in which replication fork length was "rescued" to normal levels overlapped with the conditions in which increased genotoxicity was observed. Namely, SMC5/6 depletion mitigated the fork elongation caused by APOBEC3A, but this combination also resulted in DNA damage and cell death. These data suggest that in the context of APOBEC3A activity, elongation of replication forks is protective against genotoxicity.

APOBEC3A-mediated elongation of replication forks is dependent on Primpol

Given the unexpected finding of increased replication track length upon deaminase activity, we sought to determine the mechanism by which APOBEC3A leads to elongated

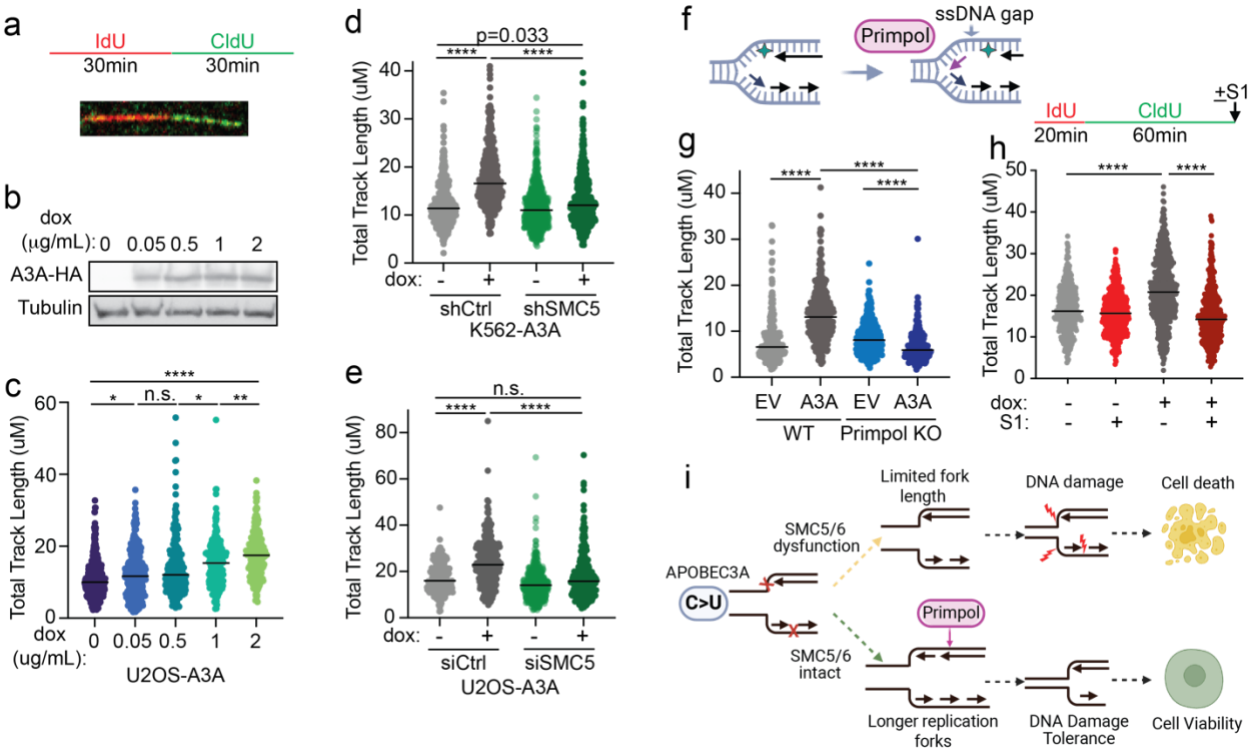

Fig 5. SMC5/6 is required for APOBEC3A-mediated replication fork elongation. (**a**) Schematic of DNA fiber assay and representative fiber tract. (**b-c**) U2OS cells were induced to express APOBEC3A with a range of dox doses. (**b**) Immunoblot shows expression of HA-tagged APOBEC3A. Tubulin is loading control. (**c**) Total track length (μM) of DNA fibers (CldU+IdU) representing complete replication tracks after expression of APOBEC3A. Bar is median. (**d-e**) Total track length (μM) of complete fibers (CldU+IdU) in K562-A3A (**d**) and USOS-A3A (**e**) cells. APOBEC3A expression was induced by dox in all cell lines. SMC5/6 was depleted by shRNA (**d**) or siRNA (**e**). Bar is median. (**f**) Schematic of replication fork lesion (green diamond) bypassed by Primpol-mediated priming (purple arrow) downstream of the lesion, leaving a ssDNA gap. (**g**) U2OS cells depleted of Primpol were compared to isogenic controls. Total track length of DNA fibers was measured after transfection of empty vector (EV) or APOBEC3A (A3A). (**h**) Total track length (μM) of complete fibers (CldU+IdU) from U2OS-A3A cells pulsed with thymidine analogues per the schematic then treated with S1 nuclease to cleave ssDNA. Bar is median. (**i**) Proposed model of APOBEC3A-induced genotoxicity enabled by SMC5/6 dysfunction. DNA fiber assays were performed in biological triplicate and analyzed by Kruskal-Wallis test. *p<0.05, **p<0.01, ****p<0.0001

replication tracks. APOBEC3A catalyzes the conversion of cytidine to uracil after which DNA glycosylases excise uracil bases, leaving an abasic site[8,9]. Abasic sites create an obstacle for replicative polymerases and lead to fork stalling. The dual primase-polymerase, Primpol, is capable of priming downstream of lesions, such as abasic sites, that block the replication machinery[59-61] (**Fig 5f**). We hypothesized that lesions generated after cytidine deamination in ssDNA may recruit DNA damage tolerance mechanisms such as Primpol-mediated obstacle "skipping." We expressed APOBEC3A or empty vector control in Primpol-knockout U2OS cells and measured replication tract length after

sequential 30 minute pulses of IdU and CldU. In wild-type U2OS cells, APOBEC3A expression resulted in a significant increase in replication track length. In isogenic Primpol-knockout U2OS cells, replication track length did not increase upon APOBEC3A expression (**Fig 5g**). These data indicate that elongation of forks upon APOBEC3A activity depends on Primpol. A Primpol-mediated repriming mechanism would leave short ssDNA gaps behind the replication fork where damaged DNA was skipped[56,62,63]. To determine whether APOBEC3A activity results in post-replicative ssDNA gap formation, we used a modified version of the DNA fiber protocol in which genomic DNA is treated with an ssDNA-specific S1 endonuclease after pulse labeling with IdU and CldU[56]. Shorter DNA fibers result upon S1 treatment if ssDNA gaps are present (**Fig 5h** schematic). Treatment with S1 nuclease led to significantly decreased DNA fiber length in cells with active APOBEC3A (**Fig 5h**). Post-replicative gaps are too small to be visualized at the resolution of DNA fiber imaging, therefore replication tracts subjected to Primpol-mediated repriming should appear longer despite containing ssDNA gaps. Our findings suggest that APOBEC3A likely does not cause an increased rate of DNA synthesis but rather causes apparent acceleration of replication when analyzed by DNA fiber analysis due to "skipping" of base lesions by Primpol.

DISCUSSION

Tumor genome sequencing has demonstrated that mutagenesis from APOBEC3A is widespread throughout human cancers[1,64], however the mechanisms that enable dysregulated activity of APOBEC3A in cancer and the impact of deamination-mediated mutagenesis on tumor cells remain elusive. While normal and abnormal regulation of APOBEC3A expression and activity are not well characterized, several genomic determinants that enhance APOBEC3A activity have been elucidated recently, including a preference for acting at T<u>C</u> dinucleotides, stem-loop structures, and ssDNA at replication forks[3,7,20,53,65-67]. The mechanisms by which cells respond to APOBEC3A activity in order to maintain genome integrity have been examined as well. The replication checkpoint, in particular ATR-Chk1 signaling, is necessary to prevent genotoxicity when APOBEC3A is active[20,21]. Additionally, loss of HMCES which covalently binds abasic sites in ssDNA, sensitizes cells to APOBEC3A-induced genotoxicity[68,69]. These prior studies

demonstrate that a variety of genome-protective responses are required to prevent cytotoxicity from APOBEC3A. In this study, we define a new mechanism of genome protection from APOBEC3A activity enacted by the SMC5/6 complex.

The SMC5/6 complex has structural and catalytic functions, all of which have been demonstrated to play roles in genome stability. The NSMCE2 subunit is an E3 SUMO ligase that SUMOylates several proteins involved in DNA replication, DNA repair, and other genome maintenance functions. NSMCE2, originally named MMS21, was identified by a screen for genetic susceptibility to alkylation damage in budding yeast[70]. Since both deamination and alkylation result in base damage, it is plausible that E3 SUMO ligase activity is required for genome stability when APOBEC3A is active. The ubiquitin ligase subunit, NSMCE1, is less well defined, but has recently been shown to target other SMC5/6 subunits particularly upon replication stress[71]. SMC5/6 DNA binding functions are also important. *In vitro*, purified yeast SMC5/6 binds to ssDNA and dsDNA through different interaction domains[24-26]. Recent data demonstrate binding of purified SMC5/6 preferentially to ssDNA-dsDNA junctions, which mimic DNA replication and repair structures[25,26]. An appealing model to explain mechanistically the synthetic lethal interaction we have uncovered between APOBEC3A activity and loss of SMC5/6 is as follows: upon damage caused at replication forks by APOBEC3A-mediated DNA deamination, binding by SMC5/6 stabilizes the fork to enable Primpol to reprime downstream of DNA lesions. Primpol activity may further enforce the need for SMC5/6 to stabilize forks due to the presence of ss-dsDNA junctions arising at post-replicative gaps (**Fig 5i**). In this model, binding of SMC5/6 is required to stabilize replication forks, and therefore in the absence of SMC5/6 binding, destabilized forks lead to DNA breaks and genotoxicity.

While SMC5/6 has multiple functions, complex formation relies on all subunits being intact[29,40,72]. Germline defects in SMC5/6 subunits associated with human diseases provide some evidence as to how loss of the complex disrupts genome stability. In the context of mammalian SMC5/6 dysfunction, several germline defects have been associated with substantial human disease. Biallelic missense mutations in NSMCE3 cause lung disease-immunodeficiency-chromosomal breakage syndrome (LICS) due to reduced complex stability[31]. Heterozygous frameshift mutations affecting NSMCE2 or

SMC5 result in primordial dwarfism and insulin resistance[30,33]. Altogether these human syndromes demonstrate that compromise of a single SMC5/6 subunit can substantially impact function of the complex. In this study, we find deleterious mutations in SMC5/6 subunits throughout human cancers which is correlated with a high mutational burden. These data raise questions regarding the etiology of mutagenesis and the sensitivity of those tumors to genotoxic agents. Interestingly, SBS10 and SBS14, signatures consistent with DNA polymerase epsilon (pol ε) dysfunction, are overrepresented in SMC5/6-mutant tumors. Experimental data in yeast suggest that SUMOylation of pol ε by SMC5/6 promotes DNA synthesis[34,73]. Thus, our findings in human cancers indicate a similar dependence of pol ε function on SMC5/6. Identification of additional mutational processes in SMC5/6-mutant tumors may provide insight into the contexts in which SMC5/6 dysfunction is permissive of mutagenesis. These studies may indicate opportunities to exploit mutagenesis in tumors with dysfunctional SMC5/6 as a therapeutic vulnerability.

Beyond SMC5/6 dysfunction in cancer, our study defines a new role for SMC5/6 pertaining to replication fork progression. Our data indicate that APOBEC3A activity results in longer replication tracks, which is somewhat counterintuitive to what would be expected of enzymatic activity that causes base damage in ssDNA. We do not interpret the DNA fiber data as demonstrating an increased rate of DNA synthesis in cells expressing APOBEC3A, rather the DNA lesions caused by deamination are being bypassed or skipped, thus forks appear to lengthen during the 60 minute integration of thymidine analogues. A prior study found that brief induction of APOBEC3A expression (30 minutes – 4 hours) led to decreased replication track lengths[69]. In contrast, our data demonstrating longer replication tracks were generated after 24-72 hours of APOBEC3A. We posit that the differences in these two findings are due to the time of genome exposure to APOBEC3A activity; initial deamination-induced damage may result in slowing of the fork but upon activation or recruitment of DNA damage tolerance pathways, the lesion can be overcome and the fork progresses. In fact, we found that fork elongation was dependent on Primpol, which may not be recruited to replication forks immediately upon deamination. In a study of cisplatin-induced replication stress, Primpol was found to be upregulated and chromatin associated following an initial dose of cisplatin which mitigated

damage when a second dose was given[60]. This may be true also for APOBEC3A in that some time is required for Primpol upregulation and recruitment.

The model we suggest raises interesting questions regarding the interaction between SMC5/6 and Primpol in DNA damage tolerance. It is possible that SMC5/6 enables or regulates Primpol activity at damaged forks due to stabilization of replication structures. Primpol was previously hypothesized to prevent mutagenesis from APOBEC3 enzymes by inhibiting error-prone polymerases at abasic sites and instead stimulating homology-directed repair (HDR) of damaged forks[74]. SMC5/6 regulates resolution of HDR intermediates during replication-associated repair[37,75], thus may be important for a Primpol-initiated repair pathway. Primpol may not be the only DNA damage tolerance mechanism that is enabled by SMC5/6. We have shown that APOBEC3A activity elicits repriming by Primpol, but it is possible that in the absence of Primpol other mechanisms compensate to maintain fork progression, such as replication fork reversal which is a bypass mechanism for abasic sites in ssDNA[76]. SMC5/6 was previously demonstrated to maintain replication forks in a conformation amenable to recombination[39], thus may be similarly important to maintain forks undergoing reversal followed by template switching. It is alternatively possible that repriming by Primpol generates an increase in ss-dsDNA junctions that elicit SMC5/6 binding for fork stabilization. In this case, it will be interesting to know whether fork damage other than cytidine deamination that elicit repriming also depend on SMC5/6 for fork stability. A non-epistatic model is also plausible, whereby Primpol and SMC5/6 may enable fork elongation independent of one another. Identification of the particular SMC5/6 function that allows fork progression upon APOBEC3A activity will undoubtedly shed light on the mechanism by which this process occurs. Modeling of SMC5/6 mutants found in human cancers may provide an opportunity to examine consequences of SMC5/6 dysfunction for replication forks under stress.

MATERIALS AND METHODS

Cell culture. HCT116-NSE4A/SMC6-mAID, a kind gift from the lab of Ian Hickson[29], U2OS-A3A, and 293T cells (used for lentiviral production) were maintained in DMEM media supplemented with 10% tetracycline-free FBS and 1% Pen-Strep. THP1, K562,

and Jurkat cells were maintained in RPMI media supplemented with 10% tetracycline-free FBS and 1% Pen-Strep. All cells were grown at 37°C in a humidified atmosphere containing 5% CO2.

Lentivectors and cell line generation. THP1-A3A, U2OS-A3A, and U2OS-C106Swere generated by lentiviral transduction as previously described[11,14,21,77]. Cas9 was introduced to THP1-A3A using lentivirus (lenti-Cas9-blast)[78]. Blasticidin (Santa Cruz) selection began 24 hours after transduction until non-transduced controls were 100% non-viable. Inducible HCT116-NSE4A/SMC6-mAID-A3A were generated by lentiviral transduction using a dox-inducible pFLRU-A3A lentivector with Thy1.2 selection marker. Following transduction, cells were bead sorted using magnetic anti-Thy1.2 beads (Miltenyi) until a stable >95% Thy1.2+ population was achieved. K562-A3A, K562-A3A*C106S, and Jurkat-A3A were generated by lentiviral transduction using the dox-inducible pSLIK-A3A lentivector with neomycin resistance as previously described[21]. All A3A transgenes have a C-terminal HA tag.

Genome-wide CRISPR-Cas9 knockout screen in THP1-A3A cells

*Brunello library lentivirus titration***.** Pooled lentivirus encoding the Brunello guide RNA library was generated as previously described[79]. To find optimal transduction conditions for an MOI of 0.3-0.5, cells were transduced with the Brunello library via spinfecting $2x10^6$ cells with a range of virus volumes. Cells were seeded in a 12-well plate at $2x10^6$ cells per well in 1 mL standard media supplemented with 10 µg/mL polybrene (Santa Cruz). Lentivirus was placed in the wells, along with a no-transduction control. The 12-well plate was centrifuged 2,000 rpm for 90 minutes at room temperature and incubated overnight.

After overnight incubation, cells were diluted 1:10 and 1:20 into four replicate plates. One plate for each dilution received 1 µg/mL puromycin. After 3 days, cells were counted to calculate transduction efficiency. Percent transduction was calculated by cell count from the dilution replicate with puromycin divided by cell count from the dilution replicate without puromycin multiplied to 100. The virus volume yielding a MOI closest to 0.4 was chosen for large-scale screening.

*Functional screen***.** Large-scale spinfection was carried out with the same conditions described above, using 12-well plates with $2x10^6$ cells per well. Each well was transduced with 50 µl Brunello library lentivirus. Wells were pooled into 15 cm plates after spinfection and overnight incubation and selected using puromycin for 7 days. Following puromycin selection, THP1-A3A-Cas9 cells were plated in triplicate into a 12-well plate at a concentration of $2x10^6$ cells per well. Doxycycline was added to +dox wells every 48 hours beginning on day 0. 400 $x10^6$ cells cultured in parallel received vehicle control (water) at equal volume. Cells from dox-treated and untreated wells were harvested on the day of dox induction and after 19 days of dox treatment. Genomic DNA was extracted using Genomic DNA mini kit (Invitrogen) on a pre-PCR bench under sterile conditions to avoid DNA contamination.

Amplification and sequencing of library gRNAs. Guide RNAs were amplified by PCR from cellular genomic DNA and amplified using one-step PCR with barcodes on reverse primers, as previously described[79]. Illumina next-generation sequencing was applied to an amplicon generated from each integrated gRNA[79]. Briefly, we used all collected gDNA (1,000× coverage) divided into 100 µL PCR reactions with 5 µg of DNA per reaction. Takara ExTaq DNA Polymerase was used with the following PCR program: [95° 2 minutes (98° 10 seconds, 60° 30 seconds, 72° 30 seconds) × 24, 72° 5 minutes]. PCR products were gel-purified using the QiaQuick Gel Extraction Kit (Qiagen). The purified pooled library was then sequenced on a HiSeq4000 with ~5% PhiX added to the sequencing lane. Quality assessment was done by qubit (for concentration), bioAnalyzer (for size distribution), and Kapa Library Quantification (for clusterable molarity).

Genome-Wide Screen Analysis. To count the number of reads associated with each sgRNA taken from the raw Fastq file, we first extracted the sgRNA targeting sequencing using a regular expression containing the three nucleotides flanking each side of the sgRNA 20 bp target. sgRNA spacer sequences were then aligned to a preindexed Brunello library (Addgene) using the short-read aligner "bowtie" using parameters (-v 0 -m 1). Data analysis was performed using custom R scripts. Using the guide sequencing data, we analyzed enrichment and depletion of gRNAs using a multi-modality algorithm

that we named CRISPRKat (**Fig S1C**) after its inventor, Katharina Hayer. Features of CRISPRKat include incorporation of several quality control measures, multiple normalization methods, and input from a variety of publicly available CRISPR screen analysis tools [Model-based Analysis of Genome-wide CRISPR/Cas9 Knockout (MAGeCK), Permutation-Based Non-Parametric Analysis (PBNPA), and Screening Bayesian Evaluation and Analysis Method (ScreenBEAM) algorithms] to identify negatively selected genes. Candidate genes are further weighted by biological variables, ultimately generating a novel scoring system used to rank genes. Table 1 shows the output only for MAGeCK version 0.5.9.5 where the counts were normalized to the 1000 non-targeting control sgRNA contained in the Brunello library.

Gene depletion by RNAi

Short-hairpin RNA. Commercially available shRNA lentiviral vectors (Sigma, TRCN0000147948, TRCN0000148162, TRCN0000147348, TRCN0000147918) were used to construct SMC5-depleted K562-A3A and Jurkat-A3A cell lines. Cells were infected with shRNA lentivirus, selected in 1 mg/mL puromycin until non-transduced controls were 100% non-viable. Of note, constitutive shRNA-mediated depletion of SMC5 was lost after 3-4 months in culture. Many vials were frozen after each cell line generation to preserve those with maximal gene depletion. Cells were only cultured for use in experiments for <8 weeks. Confirmation of gene depletion was done at least monthly while cells were in culture.

Small interfering RNA. Pooled siRNA oligonucleotides (25pmol) targeting SMC5 (Horizon SMARTpool) were transfected into $1x10^6$ cells using the RNAiMAX transfection reagent (Invitrogen) according to the manufacturer's protocol. Gene depletion was confirmed by immunoblot and/or quantitative PCR.

Antibodies. Commercially available antibodies used for immunoblotting, immunofluorescence, intracellular staining, and DNA fiber spreading were obtained from Santa Cruz Biotechnology (Tubulin, Ku86, SMC5, SMC6), GeneTex (SMC5), Novus Biologicals (Cas9 Antibody 7A9-3A3), Abcam (RPA, BrdU), Biolegend (HA), Cell

Signaling (HA, γH2AX, pChk1 S317), BD Biosciences (γH2AX-488, γH2AX-647, BrdU). Secondary antibodies for immunoblotting were obtained from Jackson ImmunoResearch (goat anti-rabbit IgG, goat anti-mouse IgG). Secondary antibodies for immunofluorescence were obtained from Invitrogen (Alexa Fluor 488 goat anti-mouse IgG, Alexa Fluor 568 goat anti-rabbit IgG). Secondary antibodies for DNA fiber spreading were obtained from Invitrogen (Alexa Fluor 488 chicken anti-rat IgG, Alexa Fluor 546 goat anti-mouse IgG).

Viability assays. To assess proportions of live and dead cells, staining was performed using the Live/Dead Kit (Invitrogen) according to the manufacturer's instructions. Data were collected using a Fortessa Flow Cytometer (BD Biosciences) or Accuri C6 Flow Cytometer (BD Biosciences) and analyzed by FlowJo software. To assess viability by metabolic activity, cells were plated in triplicate in a 96-well plate, precultured for 24 hours, then 50 μL media with and without doxycycline was added to each well every other day. 10 μL WST-8 reagent from the Cell Counting Kit-8 (Dojindo) was added to each well 4-6 hours prior to analysis using a microplate reader (BMG Labtech Omega).

Proliferation Assay. On day 0, cells were plated at a density of 200,000 cells per well in a 6-well plate. Each cell type was grown in the presence and absence of 1 mg/mL doxycycline. Cells grown in the presence of doxycycline received doxycycline doses every other day. On days 3, 5, and 7, data were collected using an automatic cell counter (Countess, ThermoFisher).

Intracellular γH2AX detection by flow cytometry*.* Cells were harvested, fixed and permeabilized using reagents from the CytoFix/CytoPerm Kit (BD Biosciences) according to the manufacturer's instructions. Cells were stained with the using a *γ*-H2AX Fluorescent Antibody (BD AlexaFluor 488 or 647 Mouse Anti-H2AX (pS139)) at a ratio of 10 μL antibody per 100 μL cells (<$1x10^6$ cells/sample). Data were collected using a Fortessa Flow Cytometer (BD Biosciences) or Accuri C6 Flow Cytometer (BD Biosciences) and analyzed by FlowJo software.

Cell Cycle Analysis. Cells were fixed in 70% ice cold ethanol, washed in PBS, and resuspended in staining solution containing Triton X, RNAseA, and 1 mg/mL propidium iodide (Biotum). Data were collected using an Accuri C6 Flow Cytometer and analyzed by FlowJo software.

Immunoblotting and Immunofluorescence. Cell lysates were prepared by harvesting cells in LDS buffer and boiling for 15 minutes, then adding 20% β–mercaptoethanol. Lysates were run on Bis-Tris gels and transferred to a nitrocellulose membrane. After incubation with primary and secondary antibodies, membranes were developed using ECL Western blotting reagents (Pierce) on a GelDoc Go system (BioRad). For immunofluorescence, cells were cultured on cover slips. Following treatment, cells were pre-extracted using 0.5% Triton-X in PBS for 15 minutes on ice to visualize chromatin-bound proteins (i.e. RPA). All other immunofluorescence experiments proceeded as followed: cells were fixed with 4% paraformaldehyde for 15 minutes at room temperature (RT), permeabilized with 0.5% Triton-X for 10 minutes at RT, and blocked with 5% BSA for 1 hour at RT. Primary antibodies were diluted in 5% BSA and incubated with slides for 1 hour to overnight. Secondary antibodies used were anti-mouse or rabbit Alexa Fluor 488 and 568 (BD Biosciences). Nuclei were visualized by 4.6-diamidino-2-phenylindole (DAPI, ThermoFisher). Images were acquired using an inverted fluorescent microscope and camera (Leica) and processed using ImageJ. Protein foci were analyzed in a blinded fashion.

Comet assay. Neutral comet assays were performed using CometAssay (Trevigen) according to the manufacturer's protocol with minor modifications as previously described[80]. In brief, cells were harvested and resuspended at $3x10^5$ cells/mL in ice cold PBS, combined with molten LMAgarose, plated onto a comet slide, and allowed to dry at 4C. Slides were incubated in lysis solution for 1 hour at 4C and then immersed in 1X TBE buffer for 30 minutes at 4C. Then slides underwent electrophoresis at 25 V for 30-45 minutes at 4C. After electrophoresis, slides were washed in DNA precipitation solution (1 M ammonium acetate, 95% ethanol) and fixed in 70% ethanol for 30 min. Fixed slides were dried overnight at RT in the dark, stained with 1X SYBR Gold (Applied Biosystems),

and washed twice with water. Images were acquired using a fluorescence microscope (Leica). Images were scored using the OpenComet plugin in ImageJ.

DNA Fiber assay. U2OS and HCT116 cells were first pulse labeled for 30 minutes with 20μM IdU, washed three times with 1X DPBS, and then pulsed with 100 μM CldU for 30 minutes. For K562 and Jurkat cells, cells were first pulsed with 20μM IdU and then flushed with 100μM CldU for 30 minutes. After pulse, cells were harvested and collected in ice cold DPBS (~1500 cells/μL). For the DNA fiber assay with the ssDNA-specific S1 nuclease (S1 Fiber), cells were permeabilized with CSK100 (100 mM NaCl, 10 mM MOPS pH 7, 3 mM $MgCl_2$, 300 mM sucrose and 0.5% Triton X-100 in water) after the CldU pulse for 10 minutes at room temperature, treated with the S1 nuclease (ThermoFisher Scientific) at 20 U/mL in S1 buffer (30 mM sodium acetate pH 4.6, 10 mM zinc acetate, 5% glycerol, 50 mM NaCl in water) for 30 minutes at 37°C, and collected in PBS-0.1%BSA with cell scraper. Nuclei were then pelleted at ~4600 x g for 5 minutes at 4°C, then resuspended in PBS (nuclei cannot be quantified, so initial number of cells plated should be considered when resuspending to a final concentration of 1,500 nuclei/μl).

To spread fibers, 2 μL of cell solution was placed on charged glass slide, mixed with 6 μL of lysis buffer (200 mM Tris-HCl pH 7.4, 0.5% SDS, 50 mM EDTA), and gravity was used to spread DNA fibers. DNA fibers were fixed in a 3:1 solution of methanol and acetic acid, denatured in 2.5M HCl for 1 hour, and blocked in previously warm 5% BSA at 37°C for 1 hour. IdU and CldU were detected using mouse anti-BrdU (1:20, Invitrogen) and rat anti-BrdU (1:75, Abcam) respectively for 1.5 hours at RT in a humid chamber followed by anti-mouse Alexa-546 (1:50) and anti-rat Alexa-488 (1:50) for 1 hour at room temperature in a humid chamber. Slides were mounted with Prolong Gold Antifade Solution (Invitrogen) and cured overnight at room temperature protected from light. Fibers were imaged with a 63X oil objective on a Leica DM4 B. Quantification and measurement of fibers was done in Image J by blinded analysis.

Native BrdU detection. Cells were plated at a density of $5x10^5$ cells per well in a 6-well plate. After one population doubling, cells were pulsed with 10 μL 10 μM BrdU (BD

Biosciences) per well. After two additional population doublings, cells were harvested, pre-extracted with 1 mL PBS with 0.2% Triton-X, and then the BD Biosciences FITC BrdU Flow Kit staining protocol was followed beginning from Step 2.

Mutational signature analysis. Mutation calls of the SMC5/6 complex genes were obtained from the Genomic Data Commons Data Portal at https://docs.gdc.cancer.gov (v.36)[81]. Those predicted to cause negative effects on the proteins' functions by either Ensembl VEP[82] or SIFT[83] were classified as deleterious mutations. Additionally, single based substitutions (SBSs) of 9493 TCGA tumors were obtained from the COSMIC database at https://www.synapse.org/#!Synapse:syn11726601/files. Tumors with one or more deleterious mutations in SMC5/6 complex were defined by merging these two datasets and were later used in downstream analysis. In contrast, other genes mutating in tumors with intact SMC5/6 complex served as control. A set of control tumors was then defined as those which carried detrimental mutations of these genes. Differences in mutational burden and APOBEC enrichment between samples were inspected and visualized using the R packages ggplot2 and tidyverse, while statistical difference was accessed by two-sided Mann-Whitney test. The R package MutationalPatterns[84] was used to study the contribution of other COSMIC SBSs signatures (v2 or v3.2).

Statistical analysis. All statistical tests were performed in R or GraphPad (Prism). Biological and/or technical triplicate tests were used to ensure robustness and reproducibility of data. Standard deviations, standard error of the mean, and p values were generated using paired and unpaired two-tail t-tests, F-tests, or Anova.

Data availability. All data presented in this manuscript are available from the corresponding author upon request.

ACKNOWLEDGEMENTS. We thank all members of the Green Lab for helpful discussions and input. We thank Stephen Sykes, Lianna Valin, Ian Hickson, and members of the Vindigni and Bednarski Labs for sharing reagents and technical support. Special thanks to Dr. Xiaolan Zhao for advice, guidance, and discussion regarding this

study. This study was funded by support from the NIH K08 CA212299 (AMG), DOD CA200867 (AMG), Cancer Research Foundation, Children's Discovery Institute, and American Cancer Society.

AUTHOR CONTRIBUTIONS. DRO, ARH, DFF, BRH, MT, RAD, AM, JHS, JD performed experiments, analyzed and interpreted data. TT and KEH performed informatic experiments and statistical tests. DRO, ARH, DFF, AMG, MDW, OS, JB, and AV conceptualized and designed experiments. AMG wrote the manuscript.

Competing Financial Interests. No disclosures or conflicts of interests were reported.

REFERENCES

1 Alexandrov, L. B., Kim, J., Haradhvala, N. J. *et al.* The repertoire of mutational signatures in human cancer. *Nature* **578**, 94-101, (2020).
2 Burns, M. B., Temiz, N. A. & Harris, R. S. Evidence for APOBEC3B mutagenesis in multiple human cancers. *Nat Genet* **45**, 977-983, (2013).
3 Nik-Zainal, S., Alexandrov, L. B., Wedge, D. C. *et al.* Mutational processes molding the genomes of 21 breast cancers. *Cell* **149**, 979-993, (2012).
4 Chan, K., Roberts, S. A., Klimczak, L. J. *et al.* An APOBEC3A hypermutation signature is distinguishable from the signature of background mutagenesis by APOBEC3B in human cancers. *Nat Genet* **47**, 1067-1072, (2015).
5 Cortez, L. M., Brown, A. L., Dennis, M. A. *et al.* APOBEC3A is a prominent cytidine deaminase in breast cancer. *PLoS Genet* **15**, e1008545, (2019).
6 Roberts, S. A., Lawrence, M. S., Klimczak, L. J. *et al.* An APOBEC cytidine deaminase mutagenesis pattern is widespread in human cancers. *Nat Genet* **45**, 970-976, (2013).
7 Jalili, P., Bowen, D., Langenbucher, A. *et al.* Quantification of ongoing APOBEC3A activity in tumor cells by monitoring RNA editing at hotspots. *Nat Commun* **11**, 2971, (2020).
8 Richardson, S. R., Narvaiza, I., Planegger, R. A., Weitzman, M. D. & Moran, J. V. APOBEC3A deaminates transiently exposed single-strand DNA during LINE-1 retrotransposition. *Elife* **3**, e02008, (2014).
9 Chen, H., Lilley, C. E., Yu, Q. *et al.* APOBEC3A is a potent inhibitor of adeno-associated virus and retrotransposons. *Curr Biol* **16**, 480-485, (2006).
10 Harris, R. S. & Dudley, J. P. APOBECs and virus restriction. *Virology* **479-480**, 131-145, (2015).
11 Landry, S., Narvaiza, I., Linfesty, D. C. & Weitzman, M. D. APOBEC3A can activate the DNA damage response and cause cell-cycle arrest. *EMBO Rep* **12**, 444-450, (2011).

12 Suspene, R., Aynaud, M. M., Guetard, D. *et al.* Somatic hypermutation of human mitochondrial and nuclear DNA by APOBEC3 cytidine deaminases, a pathway for DNA catabolism. *Proc Natl Acad Sci U S A* **108**, 4858-4863, (2011).

13 Burns, M. B., Lackey, L., Carpenter, M. A. *et al.* APOBEC3B is an enzymatic source of mutation in breast cancer. *Nature* **494**, 366-370, (2013).

14 Green, A. M., Landry, S., Budagyan, K. *et al.* APOBEC3A damages the cellular genome during DNA replication. *Cell Cycle* **15**, 998-1008, (2016).

15 Haradhvala, N. J., Polak, P., Stojanov, P. *et al.* Mutational Strand Asymmetries in Cancer Genomes Reveal Mechanisms of DNA Damage and Repair. *Cell* **164**, 538-549, (2016).

16 Baker, S. C., Mason, A. S., Slip, R. G. *et al.* Induction of APOBEC3-mediated genomic damage in urothelium implicates BK polyomavirus (BKPyV) as a hit-and-run driver for bladder cancer. *Oncogene* **41**, 2139-2151, (2022).

17 Venkatesan, S., Angelova, M., Puttick, C. *et al.* Induction of APOBEC3 Exacerbates DNA Replication Stress and Chromosomal Instability in Early Breast and Lung Cancer Evolution. *Cancer Discov* **11**, 2456-2473, (2021).

18 DeWeerd, R. A., Nemeth, E., Poti, A. *et al.* Prospectively defined patterns of APOBEC3A mutagenesis are prevalent in human cancers. *Cell Rep* **38**, 110555, (2022).

19 Petljak, M., Dananberg, A., Chu, K. *et al.* Mechanisms of APOBEC3 mutagenesis in human cancer cells. *Nature* **607**, 799-807, (2022).

20 Buisson, R., Lawrence, M. S., Benes, C. H. & Zou, L. APOBEC3A and APOBEC3B Activities Render Cancer Cells Susceptible to ATR Inhibition. *Cancer Res* **77**, 4567-4578, (2017).

21 Green, A. M., Budagyan, K., Hayer, K. E. *et al.* Cytosine Deaminase APOBEC3A Sensitizes Leukemia Cells to Inhibition of the DNA Replication Checkpoint. *Cancer Res* **77**, 4579-4588, (2017).

22 Aragon, L. The Smc5/6 Complex: New and Old Functions of the Enigmatic Long-Distance Relative. *Annu Rev Genet* **52**, 89-107, (2018).

23 Alt, A., Dang, H. Q., Wells, O. S. *et al.* Specialized interfaces of Smc5/6 control hinge stability and DNA association. *Nat Commun* **8**, 14011, (2017).

24 Yu, Y., Li, S., Ser, Z. *et al.* Cryo-EM structure of DNA-bound Smc5/6 reveals DNA clamping enabled by multi-subunit conformational changes. *Proc Natl Acad Sci U S A* **119**, e2202799119, (2022).

25 Tanasie, N. L., Gutierrez-Escribano, P., Jaklin, S., Aragon, L. & Stigler, J. Stabilization of DNA fork junctions by Smc5/6 complexes revealed by single-molecule imaging. *Cell Rep* **41**, 111778, (2022).

26 Chang, J. T., Li, S., Beckwitt, E. C. *et al.* Smc5/6's multifaceted DNA binding capacities stabilize branched DNA structures. *Nat Commun* **13**, 7179, (2022).

27 Zhao, X. & Blobel, G. A SUMO ligase is part of a nuclear multiprotein complex that affects DNA repair and chromosomal organization. *Proc Natl Acad Sci U S A* **102**, 4777-4782, (2005).

28 Ibars, E., Codina-Fabra, J., Belli, G. *et al.* Ubiquitin proteomics identifies RNA polymerase I as a target of the Smc5/6 complex. *Cell Rep* **42**, 112463, (2023).

29 Venegas, A. B., Natsume, T., Kanemaki, M. & Hickson, I. D. Inducible Degradation of the Human SMC5/6 Complex Reveals an Essential Role Only during Interphase. *Cell Rep* **31**, 107533, (2020).
30 Payne, F., Colnaghi, R., Rocha, N. *et al.* Hypomorphism in human NSMCE2 linked to primordial dwarfism and insulin resistance. *J Clin Invest* **124**, 4028-4038, (2014).
31 van der Crabben, S. N., Hennus, M. P., McGregor, G. A. *et al.* Destabilized SMC5/6 complex leads to chromosome breakage syndrome with severe lung disease. *J Clin Invest* **126**, 2881-2892, (2016).
32 Grange, L. J., Reynolds, J. J., Ullah, F. *et al.* Pathogenic variants in SLF2 and SMC5 cause segmented chromosomes and mosaic variegated hyperploidy. *Nat Commun* **13**, 6664, (2022).
33 Zhu, W., Shi, Y., Zhang, C. *et al.* In-frame deletion of SMC5 related with the phenotype of primordial dwarfism, chromosomal instability and insulin resistance. *Clin Transl Med* **13**, e1007, (2023).
34 Winczura, A., Appanah, R., Tatham, M. H., Hay, R. T. & De Piccoli, G. The S phase checkpoint promotes the Smc5/6 complex dependent SUMOylation of Pol2, the catalytic subunit of DNA polymerase epsilon. *PLoS Genet* **15**, e1008427, (2019).
35 Barlow, J. H., Faryabi, R. B., Callen, E. *et al.* Identification of early replicating fragile sites that contribute to genome instability. *Cell* **152**, 620-632, (2013).
36 Alabert, C., Bukowski-Wills, J. C., Lee, S. B. *et al.* Nascent chromatin capture proteomics determines chromatin dynamics during DNA replication and identifies unknown fork components. *Nat Cell Biol* **16**, 281-293, (2014).
37 Ampatzidou, E., Irmisch, A., O'Connell, M. J. & Murray, J. M. Smc5/6 is required for repair at collapsed replication forks. *Mol Cell Biol* **26**, 9387-9401, (2006).
38 Betts Lindroos, H., Strom, L., Itoh, T. *et al.* Chromosomal association of the Smc5/6 complex reveals that it functions in differently regulated pathways. *Mol Cell* **22**, 755-767, (2006).
39 Irmisch, A., Ampatzidou, E., Mizuno, K., O'Connell, M. J. & Murray, J. M. Smc5/6 maintains stalled replication forks in a recombination-competent conformation. *EMBO J* **28**, 144-155, (2009).
40 Potts, P. R. & Yu, H. Human MMS21/NSE2 is a SUMO ligase required for DNA repair. *Mol Cell Biol* **25**, 7021-7032, (2005).
41 Wu, N., Kong, X., Ji, Z. *et al.* Scc1 sumoylation by Mms21 promotes sister chromatid recombination through counteracting Wapl. *Genes Dev* **26**, 1473-1485, (2012).
42 Chen, Y. H., Choi, K., Szakal, B. *et al.* Interplay between the Smc5/6 complex and the Mph1 helicase in recombinational repair. *Proc Natl Acad Sci U S A* **106**, 21252-21257, (2009).
43 Agashe, S., Joseph, C. R., Reyes, T. A. C. *et al.* Smc5/6 functions with Sgs1-Top3-Rmi1 to complete chromosome replication at natural pause sites. *Nat Commun* **12**, 2111, (2021).
44 Menolfi, D., Delamarre, A., Lengronne, A., Pasero, P. & Branzei, D. Essential Roles of the Smc5/6 Complex in Replication through Natural Pausing Sites and Endogenous DNA Damage Tolerance. *Mol Cell* **60**, 835-846, (2015).

45 Torres-Rosell, J., Sunjevaric, I., De Piccoli, G. *et al.* The Smc5-Smc6 complex and SUMO modification of Rad52 regulates recombinational repair at the ribosomal gene locus. *Nat Cell Biol* **9**, 923-931, (2007).
46 Peng, X. P., Lim, S., Li, S. *et al.* Acute Smc5/6 depletion reveals its primary role in rDNA replication by restraining recombination at fork pausing sites. *PLoS Genet* **14**, e1007129, (2018).
47 Doench, J. G., Fusi, N., Sullender, M. *et al.* Optimized sgRNA design to maximize activity and minimize off-target effects of CRISPR-Cas9. *Nat Biotechnol* **34**, 184-191, (2016).
48 Lehmann, A. R. The role of SMC proteins in the responses to DNA damage. *DNA Repair (Amst)* **4**, 309-314, (2005).
49 Ju, L., Wing, J., Taylor, E. *et al.* SMC6 is an essential gene in mice, but a hypomorphic mutant in the ATPase domain has a mild phenotype with a range of subtle abnormalities. *DNA Repair (Amst)* **12**, 356-366, (2013).
50 Atkins, A., Xu, M. J., Li, M. *et al.* SMC5/6 is required for replication fork stability and faithful chromosome segregation during neurogenesis. *Elife* **9**, (2020).
51 Natsume, T., Kiyomitsu, T., Saga, Y. & Kanemaki, M. T. Rapid Protein Depletion in Human Cells by Auxin-Inducible Degron Tagging with Short Homology Donors. *Cell Rep* **15**, 210-218, (2016).
52 Hoopes, J. I., Cortez, L. M., Mertz, T. M. *et al.* APOBEC3A and APOBEC3B Preferentially Deaminate the Lagging Strand Template during DNA Replication. *Cell Rep* **14**, 1273-1282, (2016).
53 Seplyarskiy, V. B., Soldatov, R. A., Popadin, K. Y. *et al.* APOBEC-induced mutations in human cancers are strongly enriched on the lagging DNA strand during replication. *Genome Res* **26**, 174-182, (2016).
54 Wang, L., Chen, H., Wang, C., Hu, Z. & Yan, S. Negative regulator of E2F transcription factors links cell cycle checkpoint and DNA damage repair. *Proc Natl Acad Sci U S A* **115**, E3837-E3845, (2018).
55 Khan, S., Ahamad, N., Bhadra, S., Xu, Z. & Xu, Y. J. Smc5/6 Complex Promotes Rad3(ATR) Checkpoint Signaling at the Perturbed Replication Fork through Sumoylation of the RecQ Helicase Rqh1. *Mol Cell Biol* **42**, e0004522, (2022).
56 Quinet, A., Carvajal-Maldonado, D., Lemacon, D. & Vindigni, A. DNA Fiber Analysis: Mind the Gap! *Methods Enzymol* **591**, 55-82, (2017).
57 Maya-Mendoza, A., Moudry, P., Merchut-Maya, J. M. *et al.* High speed of fork progression induces DNA replication stress and genomic instability. *Nature* **559**, 279-284, (2018).
58 Techer, H., Koundrioukoff, S., Azar, D. *et al.* Replication dynamics: biases and robustness of DNA fiber analysis. *J Mol Biol* **425**, 4845-4855, (2013).
59 Quinet, A., Tirman, S., Cybulla, E., Meroni, A. & Vindigni, A. To skip or not to skip: choosing repriming to tolerate DNA damage. *Mol Cell* **81**, 649-658, (2021).
60 Quinet, A., Tirman, S., Jackson, J. *et al.* PRIMPOL-Mediated Adaptive Response Suppresses Replication Fork Reversal in BRCA-Deficient Cells. *Mol Cell* **77**, 461-474 e469, (2020).
61 Mouron, S., Rodriguez-Acebes, S., Martinez-Jimenez, M. I. *et al.* Repriming of DNA synthesis at stalled replication forks by human PrimPol. *Nat Struct Mol Biol* **20**, 1383-1389, (2013).

62 Tirman, S., Quinet, A., Wood, M. *et al.* Temporally distinct post-replicative repair mechanisms fill PRIMPOL-dependent ssDNA gaps in human cells. *Mol Cell* **81**, 4026-4040 e4028, (2021).
63 Taglialatela, A., Leuzzi, G., Sannino, V. *et al.* REV1-Polzeta maintains the viability of homologous recombination-deficient cancer cells through mutagenic repair of PRIMPOL-dependent ssDNA gaps. *Mol Cell* **81**, 4008-4025 e4007, (2021).
64 Petljak, M. & Alexandrov, L. B. Understanding mutagenesis through delineation of mutational signatures in human cancer. *Carcinogenesis* **37**, 531-540, (2016).
65 Petljak, M., Alexandrov, L. B., Brammeld, J. S. *et al.* Characterizing Mutational Signatures in Human Cancer Cell Lines Reveals Episodic APOBEC Mutagenesis. *Cell* **176**, 1282-1294 e1220, (2019).
66 Buisson, R., Langenbucher, A., Bowen, D. *et al.* Passenger hotspot mutations in cancer driven by APOBEC3A and mesoscale genomic features. *Science* **364**, (2019).
67 Langenbucher, A., Bowen, D., Sakhtemani, R. *et al.* An extended APOBEC3A mutation signature in cancer. *Nat Commun* **12**, 1602, (2021).
68 Biayna, J., Garcia-Cao, I., Alvarez, M. M. *et al.* Loss of the abasic site sensor HMCES is synthetic lethal with the activity of the APOBEC3A cytosine deaminase in cancer cells. *PLoS Biol* **19**, e3001176, (2021).
69 Mehta, K. P. M., Lovejoy, C. A., Zhao, R., Heintzman, D. R. & Cortez, D. HMCES Maintains Replication Fork Progression and Prevents Double-Strand Breaks in Response to APOBEC Deamination and Abasic Site Formation. *Cell Rep* **31**, 107705, (2020).
70 Prakash, S. & Prakash, L. Increased spontaneous mitotic segregation in MMS-sensitive mutants of Saccharomyces cerevisiae. *Genetics* **87**, 229-236, (1977).
71 Kolesar, P., Stejskal, K., Potesil, D., Murray, J. M. & Palecek, J. J. Role of Nse1 Subunit of SMC5/6 Complex as a Ubiquitin Ligase. *Cells* **11**, (2022).
72 Gallego-Paez, L. M., Tanaka, H., Bando, M. *et al.* Smc5/6-mediated regulation of replication progression contributes to chromosome assembly during mitosis in human cells. *Mol Biol Cell* **25**, 302-317, (2014).
73 Meng, X., Wei, L., Peng, X. P. & Zhao, X. Sumoylation of the DNA polymerase epsilon by the Smc5/6 complex contributes to DNA replication. *PLoS Genet* **15**, e1008426, (2019).
74 Pilzecker, B., Buoninfante, O. A., Pritchard, C. *et al.* PrimPol prevents APOBEC/AID family mediated DNA mutagenesis. *Nucleic Acids Res* **44**, 4734-4744, (2016).
75 Choi, K., Szakal, B., Chen, Y. H., Branzei, D. & Zhao, X. The Smc5/6 complex and Esc2 influence multiple replication-associated recombination processes in Saccharomyces cerevisiae. *Mol Biol Cell* **21**, 2306-2314, (2010).
76 Thompson, P. S. & Cortez, D. New insights into abasic site repair and tolerance. *DNA Repair (Amst)* **90**, 102866, (2020).
77 Everett, R. D., Parsy, M. L. & Orr, A. Analysis of the functions of herpes simplex virus type 1 regulatory protein ICP0 that are critical for lytic infection and derepression of quiescent viral genomes. *J Virol* **83**, 4963-4977, (2009).
78 Sanjana, N. E., Shalem, O. & Zhang, F. Improved vectors and genome-wide libraries for CRISPR screening. *Nat Methods* **11**, 783-784, (2014).

79 Shalem, O., Sanjana, N. E., Hartenian, E. *et al.* Genome-scale CRISPR-Cas9 knockout screening in human cells. *Science* **343**, 84-87, (2014).
80 Wood, M., Quinet, A., Lin, Y. L. *et al.* TDP-43 dysfunction results in R-loop accumulation and DNA replication defects. *J Cell Sci* **133**, (2020).
81 Grossman, R. L., Heath, A. P., Ferretti, V. *et al.* Toward a Shared Vision for Cancer Genomic Data. *N Engl J Med* **375**, 1109-1112, (2016).
82 McLaren, W., Gil, L., Hunt, S. E. *et al.* The Ensembl Variant Effect Predictor. *Genome Biol* **17**, 122, (2016).
83 Choi, Y., Sims, G. E., Murphy, S., Miller, J. R. & Chan, A. P. Predicting the functional effect of amino acid substitutions and indels. *PLoS One* **7**, e46688, (2012).
84 Manders, F., Brandsma, A. M., de Kanter, J. *et al.* MutationalPatterns: the one stop shop for the analysis of mutational processes. *BMC Genomics* **23**, 134, (2022).

SUPPLEMENTARY DATA

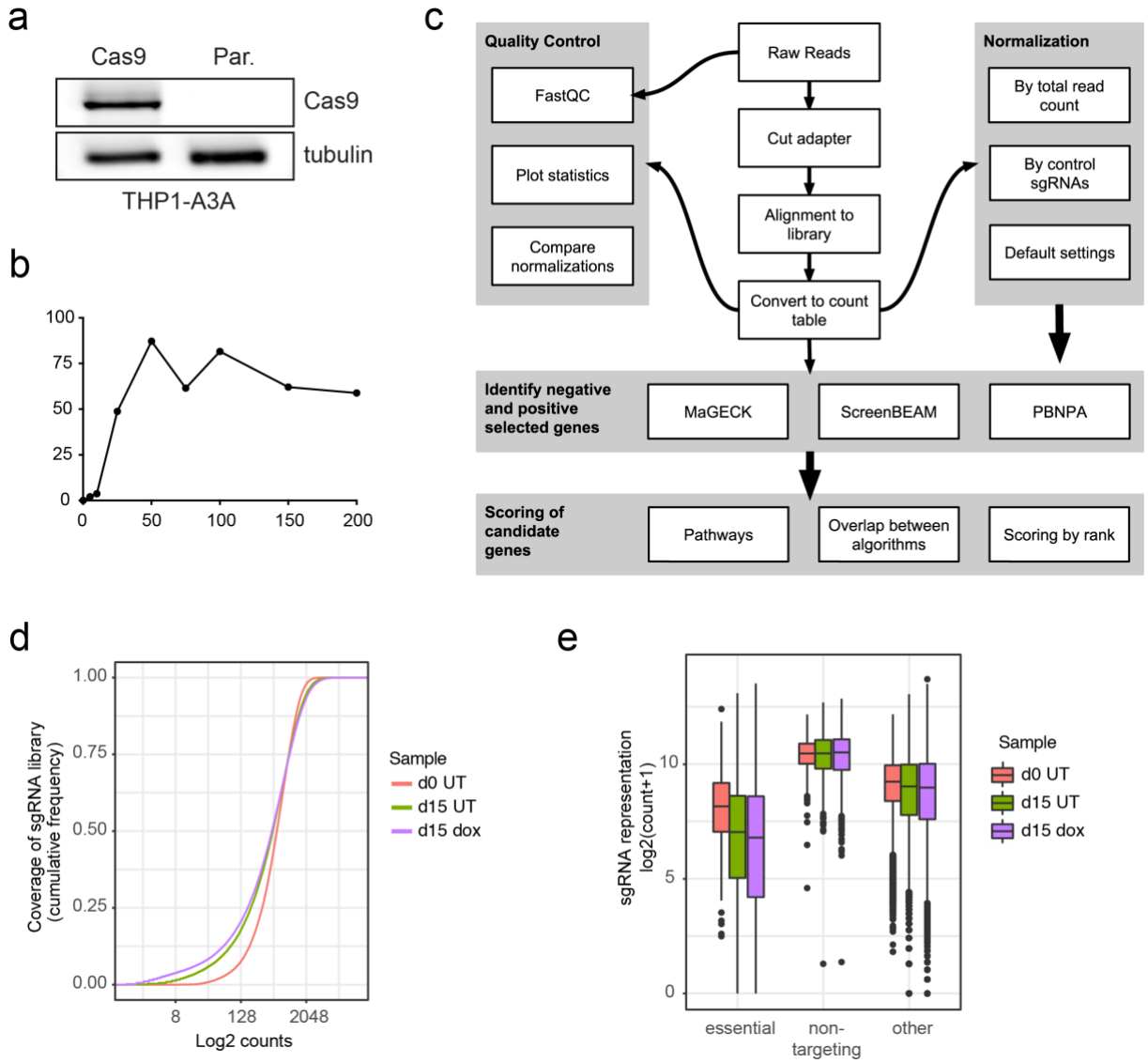

Supplementary Figure 1. CRISPR Screen Design and analysis. (**a**) A Cas9 transgene was introduced into THP1-A3A cells by lentiviral integration. Immunoblot shows Cas9 expression in transduced cells compared to parental cell line. Tubulin serves as loading control. (**b**) The Brunello sgRNA library was integrated into THP1-A3A cells by lentiviral transduction to achieve a 1:1 ratio of lentivirus to cells in order to knock out one gene per cell. Two million cells were transduced with varying volumes of concentrated library lentivirus. Transduction efficiency is estimated by number of transduced cells treated with puromycin selection compared to untreated. Screen was performed with 25 µL virus/2x10^6 cells (see Methods). (**c**) The CRISPRKat tool flowchart shows the process from raw NGS reads all the way to finished candidate gene list. Raw reads undergo quality control, trimming, and alignment to the Brunello sgRNA library. To control for varied sequence depth and batch effect, counts are normalized in several different ways and prioritized by clustering. Results are analyzed by several commonly used CRISPR screen analysis tools to generate a composite gene score for each sgRNA represented in the baseline sequencing from day 0. (**d**) Cumulative frequency of the normalized sgRNA counts for each condition sequenced. (**e**) Representation of essential gene sgRNAs and non-targeting control sgRNAs across samples.

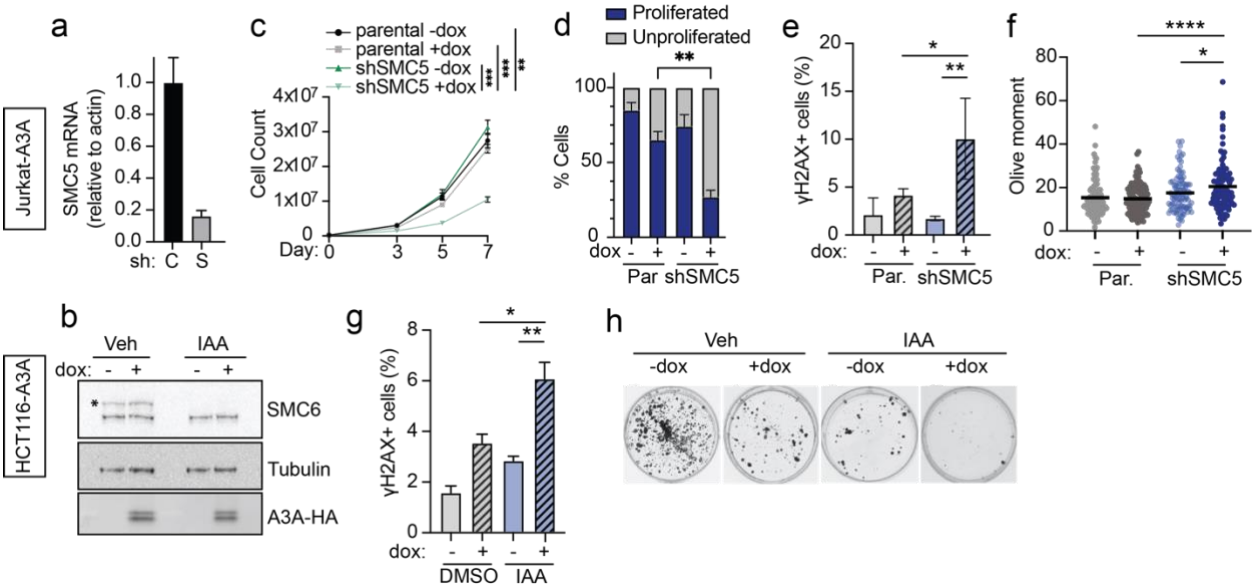

Supplementary Figure 2. SMC5/6 depletion and APOBEC3A expression result in proliferative defects and DNA damage in multiple cell types. (**a-e**) Jurkat cells engineered to express doxycycline-inducible HA-tagged APOBEC3A (Jurkat-A3A) were depleted of SMC5 (S) by integration of short-hairpin RNA (shRNA). (**a**) SMC5 transcript quantitation is compared to Jurkat-A3A cells with integrated non-targeting shRNA control (C). n=3 technical triplicate, error bars are SD. (**b**) HCT116 cells with integrated Ostir and mAID tags on endogenous SMC6 and NSE4 loci were engineered to express doxycycline-inducible HA-tagged APOBEC3A (HCT116-A3A). Cells were treated for 72 hours with indoleacetic acid (IAA) to degrade SMC6 and NSE4 and dox to induce APOBEC3A. Lysates from cells treated with IAA, dox, or combination are compared to untreated HCT116-A3A cells. Immunoblot was probed with antibodies targeting HA tag and SMC6. Asterisk (*) indicates SMC6-specific band. Tubulin was used as a loading control. (**c-f**) Jurkat-A3A cells were treated with dox every other day for 72 hours. (**c**) Cell proliferation was measured by counting cells over the course of 7 days. n=3 biological replicates, error bars are SEM, p-value by sum-of-squares F-test. (**d**) Proliferation was assessed by intracellular CFSE staining, analyzed by flow cytometry. (**e**) Flow cytometry analysis after intracellular staining for γH2AX. (**f**) Neutral comet assay to detect DSBs. For panels **d-f**, n=3 biological replicates, p-value by two-tailed t-test, error bars are SD. (**g**) HCT116-A3A cells were treated as in panel b, seeded at low density, and cultured for 2 weeks. Remaining colonies were stained with crystal violet. (**h**) Flow cytometry analysis after intracellular staining for γH2AX, n=3 biological replicates, error bars are SEM, p-value by two-tailed t-test. *p<0.05, **p<0.01, ***p<0.001, ****p<0.0001.

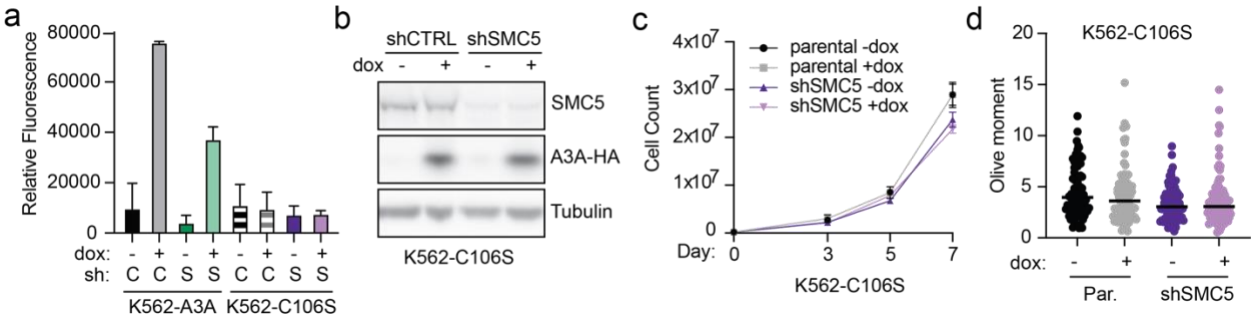

Supplementary Figure 3. Synthetic lethality is dependent on deaminase activity of APOBEC3A. (**a**) Deamination assay demonstrates C>U activity in cell lysates from K562-C106S cells in comparison to K562-A3A cells which express the catalytically active enzyme upon dox treatment. Lysates from cells with shRNA targeting control (C) or SMC5 (S). Error bars are SD. (**b**) K562 cells engineered to express doxycycline-inducible HA-tagged A3A*C106S (K562-C106S), a catalytically inactive APOBEC3A mutant, were depleted of SMC5 by RNAi (shSMC5). Immunoblot shows A3A*C106S expression after 24 hours of dox induction. Blot was probed with antibodies targeting HA tag and SMC5. Tubulin was used as a loading control. (**c**) Cell proliferation was measured by counting cells over the course of 7 days. Error bars are SEM, p-value by sum-of-squares F test. (**c**) Intracellular staining and flow cytometry analysis of γH2AX in K562-C106S cells. N=3 biological replicates, error bars are SEM. (**d**) Neutral comet assay to detect DSBs, bar is median, error bars are SD. All assays represent results of three independent biological replicates.

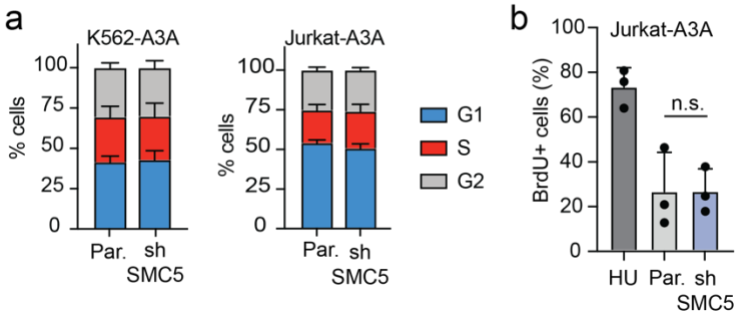

Supplementary Figure 4. Cell cycle is not impacted by SMC5/6 depletion. (**a**) K562-A3A and Jurkat-A3A cells were depleted of SMC5 by RNAi, stained with propidium iodide, and analyzed for cell cycle profile by FACS. n=3 biological replicates. (**c**) Native BrdU staining was performed on Jurkat-A3A cells. Cells were pulsed with BrdU for 36 hours. Intracellular staining with anti-BrdU antibody was analyzed by flow cytometry. P-value by two-tailed t-test, n=3 biological replicates, bars are mean with SD. HU-treated Jurkat cells serve as positive control.

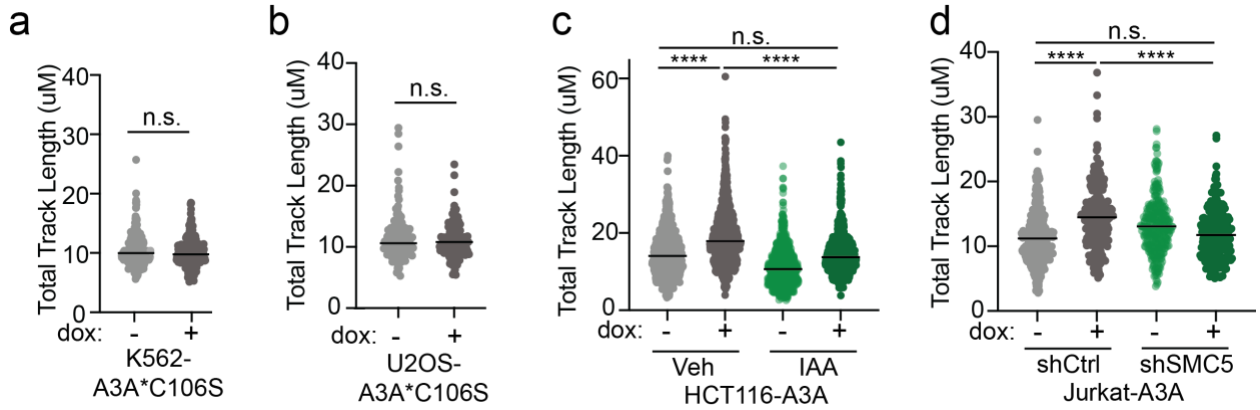

Supplementary Figure 5. APOBEC3A-mediated replication fork elongation depends on catalytic activity. Total track length (μM) of DNA fibers from K562 (**a**) and U2OS (**b**) cells induced with dox for 72 hours to express catalytically inactive APOBEC3A (A3A*C106S). (**c-d**) Total track length (μM) of DNA fibers in HCT116-A3A and Jurkat-A3A cells. APOBEC3A expression was induced by dox for 72 hours. SMC5/6 was depleted by IAA treatment for 72 hours (**c**) or shRNA (**d**). Bar is median, p-value by Kruskal-Wallis test. ****p<0.0001